Arabian Journal of Chemistry (2021) **14**, 103251

King Saud University

Arabian Journal of Chemistry

www.ksu.edu.sa
www.sciencedirect.com

ORIGINAL ARTICLE

Zinc oxide nanoparticles fabrication using *Eriobotrya japonica* leaves extract: Photocatalytic performance and antibacterial activity evaluation

Arif Nazir [a,*], Ali Akbar [a], Hanadi B. Baghdadi [b,c], Shafiq ur Rehman [a], Eman Al-Abbad [d], Mahvish Fatima [e], Munawar Iqbal [a], Nissren Tamam [f,*], Norah Alwadai [f], Mazhar Abbas [g]

[a] *Department of Chemistry, The University of Lahore, Lahore, Pakistan*
[b] *Department of Biology, College of Sciences, Imam Abdulrahman Bin Faisal University, P.O. Box 1982, 31441 Dammam, Saudi Arabia*
[c] *Basic and Applied Scientific Research Center, Imam Abdulrahman Bin Faisal University, P.O. Box 1982, 31441, Dammam, Saudi Arabia*
[d] *Department of Chemistry, College of Science, Imam Abdulrahman Bin Faisal University, P.O. Box 1982, Dammam 31441, Saudi Arabia*
[e] *Department of Physics, Deanship of Educational Services, Qassim University, Buraydah, Saudi Arabia*
[f] *Department of Physics, College of Sciences, Princess Nourah bint Abdulrahman University (PNU), Riyadh 11671, Saudi Arabia*
[g] *Department of Biochemistry, University of Veterinary and Animal Sciences, Lahore (Jhang Campus), Jhang 35200, Pakistan*

Received 19 February 2021; accepted 1 June 2021
Available online 6 June 2021

KEYWORDS

Nanoparticles;
Green synthesis;
Plant mediated;
Photocatalytic;
Antibacterial;
Antioxidant activity

Abstract In the present investigation, ZnO NPs was fabricated using *Eriobotrya japonica* leaves extract. The *E. Japonica* leaves powder was extracted and mixed with 0.2 *M* zinc nitrate in 2:4 ratio and pH was adjusted using ammonia solution. Different techniques including UV–Visible spectroscopy (U.V-Vis), X-ray diffraction (XRD), Energy dispersive X-ray (EDX), Fourier transform infrared (FTIR) and Scanning electron microscope (SEM) techniques were employed to characterize the synthesized ZnO NPs. The peak at 375 nm was observed for ZnO NPs, while the average particle size was 13.0 nm. The elemental composition analysis revealed the NPs was highly pure having irregular platelets shape with aggregates tendency. The as-prepared ZnO NPs was analyzed for their photocatalytic, antibacterial and antioxidant properties. The ZnO NPs exhibited a promising DPPH scavenging activity and was highly active against *S. aureus, P. multocida, E. coli* and

* Corresponding authors.
E-mail addresses: anmalik77@gmail.com (A. Nazir), Nmtamam@pnu.edu.sa (N. Tamam).
Peer review under responsibility of King Saud University.

Production and hosting by Elsevier

https://doi.org/10.1016/j.arabjc.2021.103251

B. subtilis strains. The photocatalytic activity (PCA) was appraised against the removal of methylene blue (MB) dye and we found 72% degradation within 160 min of treatment. Since the synthesized NPs have shown promising bioactivity and PCA, the synthesis of these NPs using *E. japonica* leaves extracts is suggested for different applications.

1. Introduction

Nanotechnology provides a progressive pathway for innovative development that concern with material at nanoscale. Nanoparticles show very unique and enhanced physicochemical properties due to their sizes at nanoscale. The nanomaterials have been proved to be highly efficient in catalytic application in diverse fields (Awwad et al., 2021a; Chen et al., 2021; Khan et al., 2020, 2019; Li et al., 2021; Mathew et al., 2020; Mukhtar et al., 2019; Numrah et al., 2019). A range of state-of-arts like carbon dots, nanotubes, magnetic NPs, nanorods, nanoflowers, nanorods, nano-rings, nanowires, nano-walls, nanospheres and core–shell structures etc. have been prepared using different techniques (Chundattu et al., 2016; Jabeen et al., 2019; Jamila et al., 2020; Kamran et al., 2019). Interestingly, the applications of nanomaterials depend on specific size, dimensions and physical properties and researchers used different strategies to enhance the chemical and physical properties, which include chemical, physical and biological approaches (Arshad et al., 2018; Ismail et al., 2021; Jamil et al., 2020; Sohail et al., 2020). The physical approaches include vapor deposition, laser ablation, microwave-assisted, sono-chemical reduction, gamma radiation-assisted and arc discharge, while chemical approaches includes polyol route, electrochemical, micro-emulsion and thermal decomposition etc. (Sanda et al., 2021; Sönmezoğlu et al., 2014). On the other hand, biological methods are either plant or microbe facilitated. Preparation of metal NPs via biological approach is very economical in term of energy, reaction time, safety, simplicity and yield of the product (Yedurkar et al., 2016). Before, different biological agents were employed for the fabrication of ZnO NPs, which showed promising photocatalytic and biological activities (Table 1). *E. japonica* (also known as Loquat locally) belongs to *Rosaceae* family. It has been generally employed as a medicinal material in Asian countries for chest related problems. Phytochemical analysis revealed the presence of many useful compounds including terpanes, flavonoid, tannin, glycoside and essential oil in *E. japonica* extracts (Li et al., 2020). However, the extract can be further employed for the fabrication of NPs.

So far, the green synthetic approaches gained much attention due to their eco-benign nature (Al Banna et al., 2020; Awwad et al., 2020b; Igwe and Nwamezie, 2018; Remya et al., 2017; Shammout and Awwad, 2021). On the other hand, the population growth, water resources contamination, climate change demands the green and clean approaches to avoid the environmental issues. Among water pollution sources, the textile industry is one of major contributors, hence, there is need to remediate dyes in effluents to ensure the environmental integrity is an important concern of the present rea (Golmohammadi et al., 2020). The dyes are considered damaging to the breathing organisms due to their poisonous characteristics. It is indispensable to remove these dyes from any source including wastewater. Out of the various approaches, photocatalysis is one of major and most valid approach for removal of dyes through the process of degradation. The NPs prepared via green route showed excellent photocatalytic activity for the elimination of dyes. Earlier studies stated that NPs synthesized via green route have been studied for their PCA and biological profiling and responses were promising, i.e., sea buckthorn fruit was used for the synthesis of NPs and used as a photocatalysts for the elimination of malachite green, eosin yellow, congo red and methylene blue dyes and up to 99% degradation was achieved under UV light irradiation (Rupa et al., 2019). Similarly, Murex plant juice was employed for synthesis of NPs and exhibited excellent photocatalysis against MB dye under UV (Babitha et al., 2019) and the ZnO prepared using *C. ramiflora* also exhibited PCA for the removal of RhB, which was 98% in 200 min under UV (Varadavenkatesan et al., 2019). To date, the ZnO NPs have been prepared from these plants, i.e., Olea europaea, *C. sinensis,* M. oleifera, E. globulus, A. indica, R. officinalis, O. basilicum, C. gigantea, H. sabdariffa, C. procera, P. odorifer, S. torvum, G. wallichianum, A. Sativum, L. esculentum, C. papaya, A. esculentus, C. sinensis, C. aurantifolia, C. woodsonii and S. glauca (Weldegebrieal, 2020). Based on literature survey, The *E. japonica* has not been investigated for the fabrication of ZnO NPs.

Hence, this investigation was undertaken to fabricate ZnO NPs using *E. japonica* leaves extract. The synthesized NPs were studied for physico-chemical properties using EDX, XRD, FTIR, SEM and UV–vis techniques. The antibacterial (*S. aureus, P. multocida, E. coli* and *B. subtilis* strains), antioxidant (TPC, DPPH and TFC) and photocatalytic activities was also evaluated. The catalytic performance was evaluated against MB dye under UV irradiation.

2. Material and methods

The study was conducted for the fabrication and characterization of ZnO NPs using analytical grade chemicals. These were acquired from Sigma Aldrich. The fresh *E. Japonica* plant leaves were obtained from fields, when plants started flowering. Leaves were collected from same plant at different branches from Choa saidan shah. The leaves were washed with deionized water, which were dried under shadow. The dried leaves were pulverized to obtained fine particles. The powder was kept in an air tight container for further use.

2.1. Extract preparation

The leaves powder (20 g) was mixed with deionized water (100 mL). The mixture was heated for 60 min at 80 ℃ with continues stirring. Finally, extract is cooled down to 25 ℃ and filtered. The filtrate was kept at 4 ℃ and employed for subsequent NPs fabrication.

2.2. Preparation of ZnO NPs

The zinc nitrate solution (0.2 *M*) was prepared in deionized water. Now, the zinc nitrate solution was mixed with *E. Japonica* leaf extract (2:4 ratio) in 250 mL conical flask. The mixture is heated with constant stirring for 10 min at 60 ℃. The pH level of the mixture was adjusted using NaOH (2 *M*) until pH reached to 12 and stirred for 150 min (Conter checked it is ok). The obtained precipitates were separated by centrifuging at 5000 rpm, which was washed with water and ethanol many times. The synthesized NPs were kept at 60 ℃ in an oven overnight for drying. For characterization and PCA, the NPs were calcined at 300 ^{0}C for 2 h and for biological activity, the NPs were dried at 80 ^{0}C for 2 h.

Table 1 Summary of plants that are utilized for the fabrication of ZnO and their applications.

S. No	Plants	Parts	Particle size and shape	Functional groups	Applications	References
1	*Z. jujube*	Fruit	21–37 nm, spherical	Hydroxyl, carboxyl, carbonyl	Photocatalytic activity (PCA)	(Golmohammadi et al., 2020)
2	*Z. nummularia*	Leaves	12.47–26.97 nm, spherical	Hydroxyl, alkyne, amine,	Antifungal activity (ANA)	(Padalia and Chanda, 2017)
3	*Z. mays*	Peel	300–550 nm, flowers	Alkene, hydroxyl, ether,	Antibacterial activity (ABA)	(Quek et al., 2020)
4	*S. cumini*	Leaves	64–78 nm, spherical	Amide, hydroxyl	PCA	(Rafique et al., 2020)
5	*S. baicalensis*	Roots	50 nm, spherical	Hydroxyl, alkene, alkane	PCA	(Chen et al., 2019)
6	*Quince seed*	Mucilage	25 nm, spherical	Hydroxyl	PCA	(Tabrizi Hafez Moghaddas et al., 2020)
7	*P. caerulea L.*	Leaves	70 nm, spherical	Alkene, amide, amine, carbonyl, alkyl halide, alkane	ABA	(Santhoshkumar et al., 2017)
8	*L. esculentum*	Peel	9.7 nm, Polyhedral	Aromatic rings	PCA	(Nava et al., 2017)
9	*L. nobilis*	Leaves	20–30 nm, Spherical and hexagonal	Hydroxyl, amine, alkene, alkane, carboxyl	PCA	(Chemingui et al., 2019)
10	*L. nobilis*	Leaves	20–30 nm, Spherical and hexagonal	Hydroxyl, alkane, amine, alkene, carboxyl	ABA	(Chemingui et al., 2019)
11	*J. regia L.*	Leaves	45–65 nm, Spherical	Hydroxyl, alkene, alkane	ABA	(Darvishi et al., 2019)
12	*C. citratus*	Leaves	6.6–42.9, spherical	Amide, hydroxyl	PCA	(Sidik et al., 2020)
13	*C. sinensis*	Peel	9.7 nm, Polyhedral	Aromatic rings	PCA	(Nava et al., 2017)
14	*C. colocynthis (L.)*	Fruit, seed and pulp	20–100 nm, Irregular polygon, flowers, Hexagonal	Hydroxyl, alkane, carbonyl	ABA	(Azizi et al., 2017)
15	*J. sambac*	Leaves	13.4 nm, platelets, irregular	Hydroxyl, alkane, carbonyl	PCA, ABA	Present study

2.3. Characterization

We have prepared ZnO NPs using plant extract and then these NPs was further characterized by using various advanced techniques including UV–visible, XRD, FTIR, SEM and EDX techniques. The Schimadzu UV-1800 (spectrophotometer) was employed for UV–visible analysis and Agilent Cary 630 was used for FTIR analysis. The structure and fundamental arrangement were investigated by SEM analysis by employing Nova Nano SEM 450 and XRD analysis was performed with the help of instrument named as Philips-x pert PRO 3040/60 (diffractometer) at 298 K in range 2θ = 20-80° using Cu Kα (λ = 0.15405 nm). Scherer's formula given in Eq. (1) was applied for crystallite size determination.

$$D = \frac{K\lambda}{\beta\cos\theta} \quad (1)$$

where 'D' denotes size, 'K' is constant equal to 0.99, "λ" is wavelength, "β" = full width at half maximum and "θ" = Bragg angle.

2.4. Evaluation of PCA of ZnO NPs

Fig. 1 demonstrates the PCA of NPs examined by removal of MB dye under the effect of UV irradiations. The lamp of mercury, 500 W was employed as a UV light source (intensity 100 mW/cm^2). For the procedure to carry out, 15 mg catalyst and MB dye solution (10 mg/L; 50 mL) was assorted. The

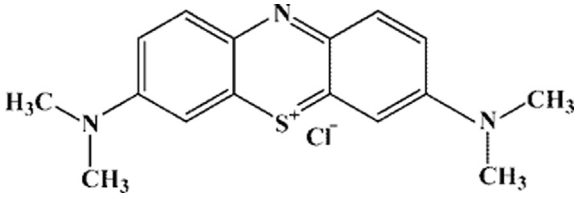

Fig. 1 Structure of MB dye used for PCA evaluation of ZnO NPs.

mixture was agitated for half an hour in dark to obtain equilibrium and furthermore, it was irradiated with UV light for 160 min. During this procedure, the stirring was continuously performed. 2 mL solution was withdrawn after certain regular time interval. It was then filtered and concentration was assessed at 660 nm. The efficiency (%) was calculated by employing Eq. (2). Where, C_0 and C_f are the absorbance values before irradiation and at time "t", respectively.

$$Degradation(\%) = \left[\frac{C_0 - C_f}{C_0}\right] * 100 \quad (2)$$

2.5. Evaluation of antibacterial activity (ABA)

The ABA of ZnO NPs was appraised versus a set of bacterial strains. Fresh cultures of bacterial strains were prepared using nutrient broth as culture media. All cultures were stored at 4 ℃

and spores (1.2×10^8 CFU/mL) were used. Nutrient Agar media was prepared and sterilized the media by autoclaving the media at 121 ℃ for 15 min. Wick's paper discs as a loading agent of ZnO NPs were prepared of 9 mm size and were also sterilized and then prior to the transfer of medium to petri plates; inoculums of different bacterial strains (100 µL/100 mL) were added to the warm agar medium and mix it for homogeneity of bacterial culture with media. Then (20 mL) nutrient agar media were poured in each petri plates and left for solidification of media, for preparation of uniform bed of media in petri plates, avoid to shaking the plates. Then, 500 µL of ZnO NPs (10 mg/L) in 10 to 40 mg/mL range was loaded on disc. These discs were then dried for further use. By using sterile forceps, discs containing different concentration of controls and ZnO NPs were laid down on media plates marks them. Rifampicin with the concentration of 10 mg/mL was kept a control (positive control for comparison). The petri plates were placed for 24 h at 37 ℃. The ZnO NPs displayed ABA by inhibiting the bacterial growth. All the tests were run in a set of three runs and data obtained was calculated as a mean and SD (Brudzynski and Kim, 2011).

For the estimation of MIC of ZnO NPs, a 96 well plate's method was used in aseptic environment. In 96 well plate, ZnO NPs 100 µL in 10–40 mg/mL concentration range were poured into the first row of the plate and nutrient broth (50 µL) was added in all other wells, and 50 µL of (Zno NPs) from first well transferred into next wells and then serial dilutions of tested (Zno NPs) were performed. Resazurin indicator (10 µL) was supplied in each well. Later, bacterial suspension (10 µL with $5x10^6$ CFU/mL) were transferred. A positive control (antibiotic) was run in parallel to the sample. Plates were covered to avoid dehydrated and plates were kept for 24 h at 37 °C. Elisa reader was used to measure absorbance at 500 nm. Any color change (observed) at most diluted concentration was observed taken as least inhibitory concentration value (Sarker et al., 2007).

2.6. Evaluation of antioxidant activity (AOA)

The AOA was appraised by DPPH (2, 2-diphenyl-1-picryl hydrazyl) test following method reported elsewhere (Bozin et al., 2006). The scavenging effect (%) was measured using Eq. (3). The assay was carried out in a set of three runs and data was averaged.

$$DPPH\,scavaning(\%) = \left[\frac{A_c - A_s}{A_c}\right] * 100 \quad (3)$$

where A_C and A_s are the absorbance value of the control and sample, respectively. Total phenolic contents (TPC) was determined by standard method, with some modification by using Folin-Ciocalteu reagent (Abbas et al., 2019). Different concentration of ZnO-NPs, 10–40 mg/mL were prepared as a stock solution. From each stock solution, transfer 300 µL of different concentration into sterilized test tube and then, Folin-Ciocalteu reagent (500 µL) was poured and homogenized well. Then, Na_2CO_3 (1 mL, 800 mM) was mixed and the suspension is kept at room temperature for 2 h. Before absorbance measurement, whole contents again vortex and then transfer to 400 µL sample from each test tube and absorbance was determined at 765 nm. Gallic acid as a standard was used to estimate the TPC employing a calibration curve and outcome is presented as µg of gallic acid equivalent (GAE) per gram of ZnO NPs of dry matter. Total flavonoids contents (TFC) of green synthesized nanoparticle of ZnO NPs using their different concentration (10 to 40 mg/mL) were measured and their obtained data was documented as microgram of Catechin equivalents (CAE) per g of sample. A freshly reaction reagents such as 5% Na_2NO_3, 10% Al_2Cl_3 and 1 M NaOH were also prepared. Transfer 1 mL of ecofriendly ZnO NPs into new test tube and added 400 µL of 5% Na_2NO_3 mix well for homogeneity, after this then diluted the mixture by adding 6 mL of distilled water. After 5 min incubation then added, 700 µL of 10% Al_2Cl_3 and 3 mL of 1 M NaOH and absorbance was noted at 510 nm (Sakanaka et al., 2005).

3. Results and discussion

3.1. UV–Visible and FTIR analysis

The UV–Vis analysis of ZnO NPs was performed, results are depicted in Fig. 2 and a band at 375 nm exposed the presence of ZnO NPs. The absorption of radiant energy is an essential for a photocatalyst to carry out the photocatalytic reaction. The ZnO displayed a higher captivation capacity in the UV light range. Previous studies also revealed similar observation that pure ZnO is active UV light (Mahmud et al., 2020). The FTIR is used to find the presence of bioactive functional groups attached with the NPs. In FTIR analysis (Fig. 3), the bands were observed at 3505, 1560, 1507, 1388, 1034 and 885 (cm^{-1}). The band at 3505 cm^{-1} corelates to the O-H stretching and a band at 1560 cm^{-1} is due to the aromatic C = C group (Awwad et al., 2020a). The C-C (aromatic) was recorded 507 cm^{-1}. The band at 1388 cm^{-1} is due to C-H vibration functional group. The C-N (aliphatic amine) was detected at 1034 cm^{-1} and a band at 885 cm^{-1} is due to the C-H (aromatic) group. The FTIR analysis of extracts was also performed and the functional groups detected in NPs was also found to be in the extract used for ZnO NPs preparation (Fig. 4).

3.2. Morphology and elemental composition

The morphology of ZnO NPs synthesized via green route was examined by SEM analysis. SEM gave the evidence of surface characteristics of NPs and any interaction between ZnO NPs

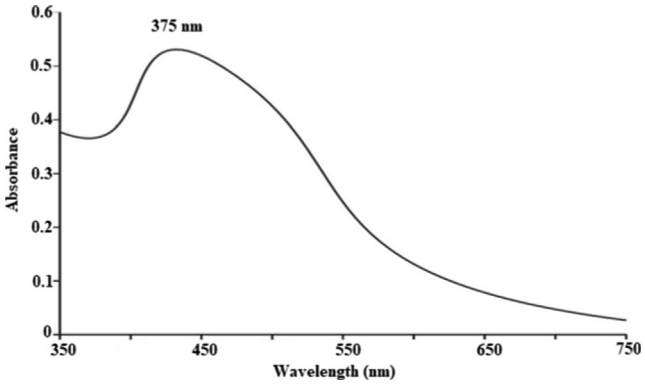

Fig. 2 UV–Visible response of Zn NPs synthesized fabricated by employing *E. japonica* leaves extract.

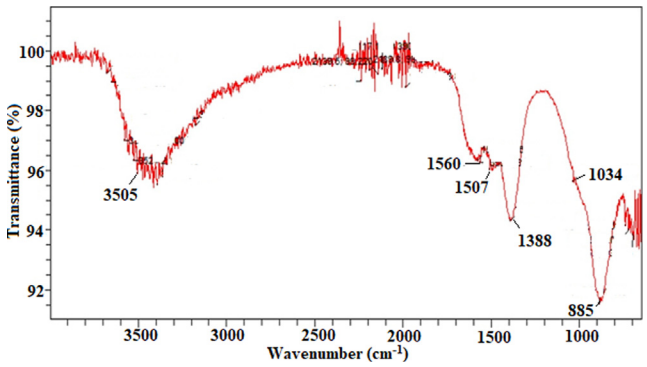

Fig. 3 FTIR analysis of ZnO NPs fabricated by employing *E. japonica* leaves extract.

and bioactive agents. The response of SEM analysis is depicted in Fig. 5. The ZnO particles was in the form of platelets and irregular in shape. Moreover, the ZnO NPs were in aggregates form, which is due to the interface among biomolecules caping and stabilizing the NPs. Elemental analysis of the prepared ZnO NPs was also performed for the assessment of purity and composition of the prepared ZnO NPs and response is depicted Fig. 6. The oxygen and zinc were detected in the prepared sample with 19.87 and 74.95 (%) ratio, which indicates that ZnO NPs are highly pure.

3.3. Structural analysis

The size and crystallinity of the ZnO NPs was determined by XRD analysis and responses thus observed are presented in Fig. 7. The ZnO NP was face centered cubic (FCC) crystals with (1 0 0), (0 0 2), (1 0 1), (1 0 2), (1 1 0), (1 0 3) and (1 1 2) planes, which is in line with the standard (JCPDS # 36–1451) (Jamdagni et al., 2018). The Scherer formula was employed to approximate the particles size of ZnO NPs.

$$Particle\ size\ (nm) = \frac{k\ddot{e}}{\hat{a}Cos\grave{e}} \quad (4)$$

where k is constant having value 0.9, λ (0.15406 nm) is the wavelength of x-ray, β is the full width at half maximum (FWHM) value in radians and θ is the half of the diffraction angle of the middle of the peak in radians. By using the Scherrer equation, the ZnO NPs size was found to be 13 ± 4.2 nm. These conclusions are harmonized with previous reports, which utilized green routes (using plant extracts) for the preparation of ZnO NPs at nano-scale having different shapes, i.e., *Z. jujube* fruit extract are utilized for the successful fabrication of ZnO NPs, which furnished 21–37 nm and spherical shaped NPs (Golmohammadi et al., 2020). Similarly, *Z. nummularia* leaves extract furnished ZnO NPs in 12.47–26.97 nm range having spherical shape (Padalia and Chanda, 2017). Also, *Z. mays* peel furnished 300–550 nm sizes particle with flowers like morphology (Quek et al., 2020). The ZnO NPs formation mechanism is displayed in Fig. 8. It is proposed that the Zn ions reduced to zero valent atom by reacting with electron rich compounds in the extracts. First, a $Zn(OH)_4^{2-}$ specie is formed in basic pH, which on reaction with polyphenols and flavonoids form a complex, which on calcination and decomposition furnished ZnO NPs (Chemingui et al., 2019).

3.4. Photocatalytic activity

The PCA of ZnO NP was scrutinized by removing MB dye under the impact of UV irradiation and the PCA response of ZnO NPs was highly promising. A peak at 681 nm decreased quickly with irradiation time, which show the removal of MB dye (Fig. 9). The dye removal was recorded to be 18, 32, 41, 50, 62 and 72 (%) for the irradiation time of 5, 10, 20, 40, 80 and 160 (min), respectively. The enhanced dye degradation is corelated with generation of highly reactive species on irradiation of ZnO NPs, like hydroxyl radical, which degrade the dye oxidatively to low molecular moieties. The degradation mechanism is presented in Eqs. (5)–(9). On irradiation, an e^- and h^+ pair is formed by excitation of electrons from VB to CB. The e^- (CB) reacts with oxygen to produce superoxide radical and h^+ react with water to produce hydroxyl radical. The hydroxyl radical are reactive species that degrades the

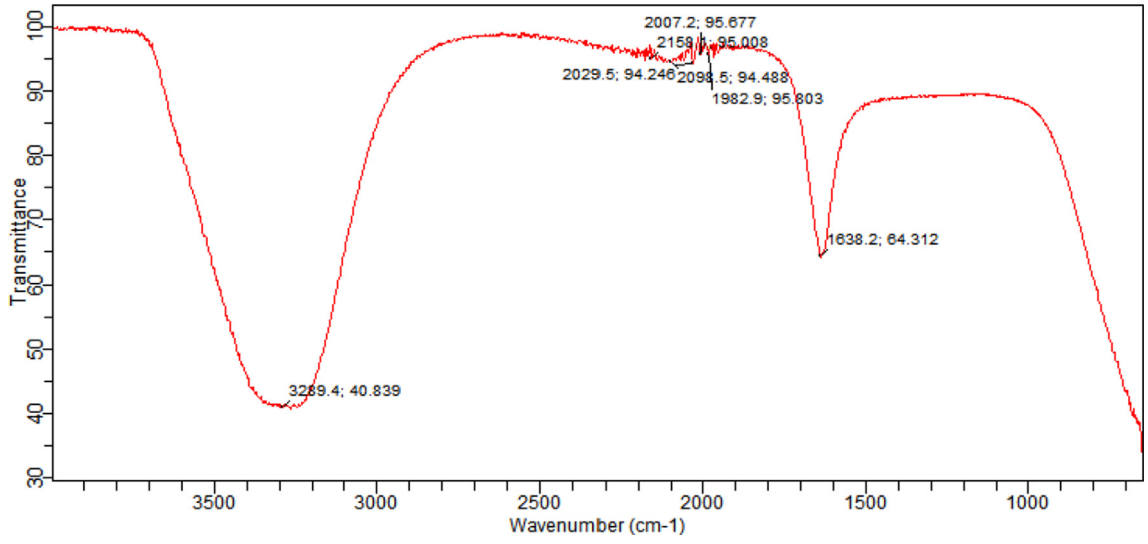

Fig. 4 FTIR analysis of *E. japonica* leaves extract used for the synthesis of ZnO NPs.

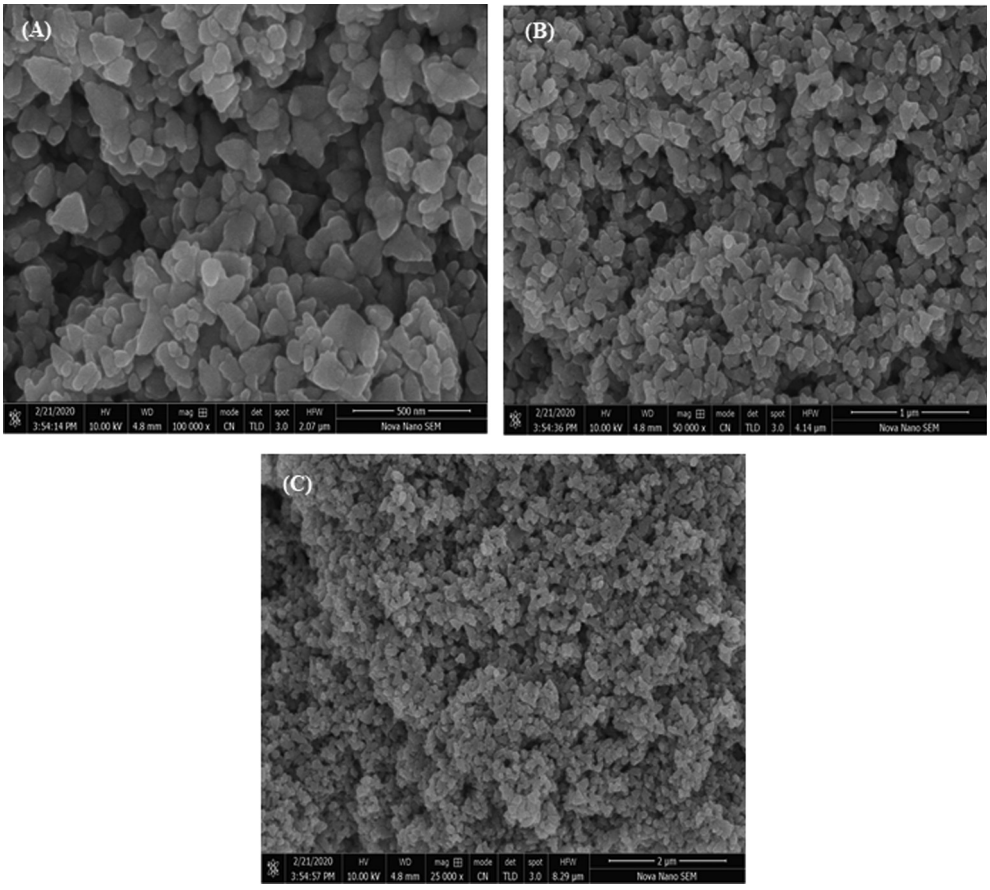

Fig. 5 SEM images at of ZnO NPs fabricated using *E. japonica* leaves extracts.

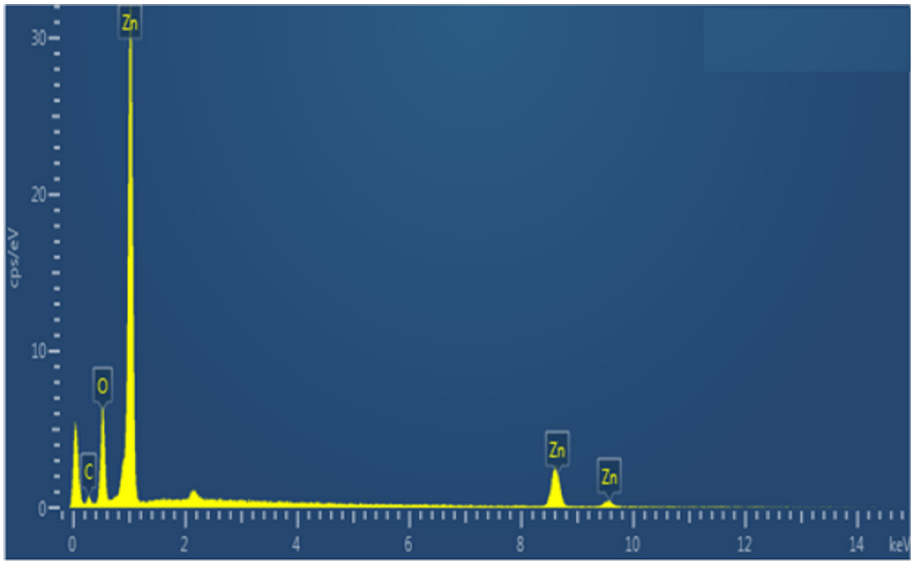

Fig. 6 EDX spectrum of ZnO NPs fabricated using *E. japonica* leaves extracts.

MO dye oxidatively into intermediate of low molecular weight and finally, in to H_2O, CO_2 and inorganic ions (Eqs. (5)–(9)). The PCA of CuO NPs was auspicious for the removal of MO dye under the exposure of visible light, which is considered economical for the redress of MB dyes. Also, previous studies support the findings of the present investigation regarding fabrication of ZnO via eco-benign approaches and their promising PCA, i.e., *jujube fruit* extract was employed for the fabrication of ZnO NPs, which were studied employing TEM, XRD, FTIR, SEM and EDX techniques. The ZnO NPs were

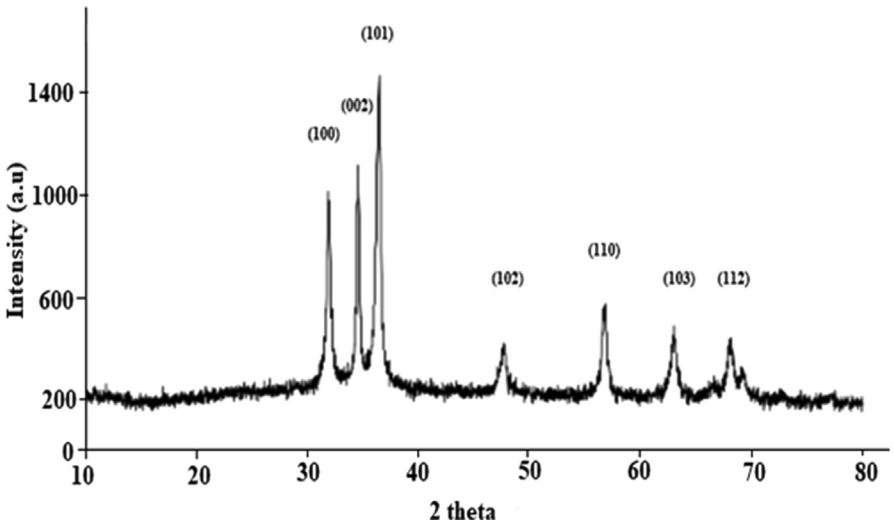

Fig. 7 XRD pattern of ZnO NPs fabricated using *E. japonica* leaves extracts.

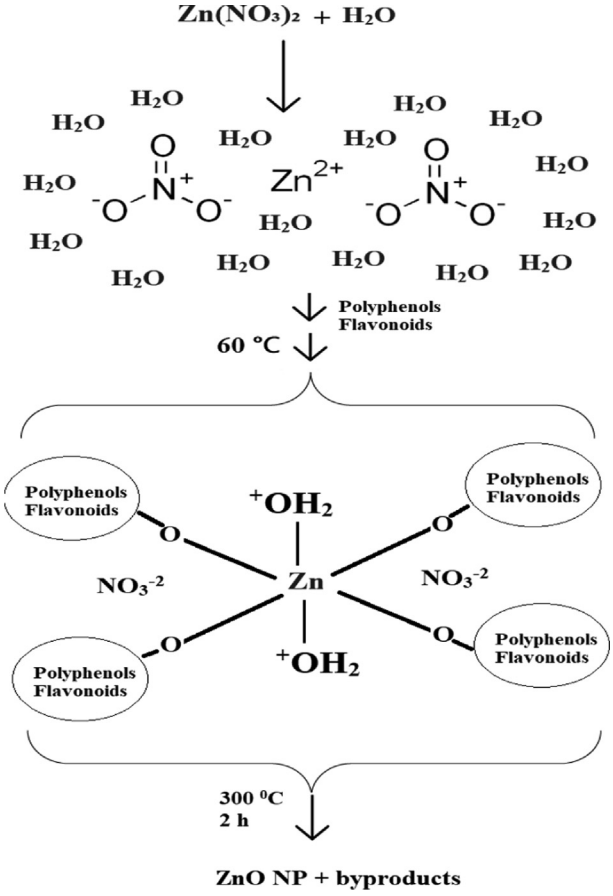

Fig. 8 Proposed ZnO NPs formation mechanism using *E. japonica* leaves extract.

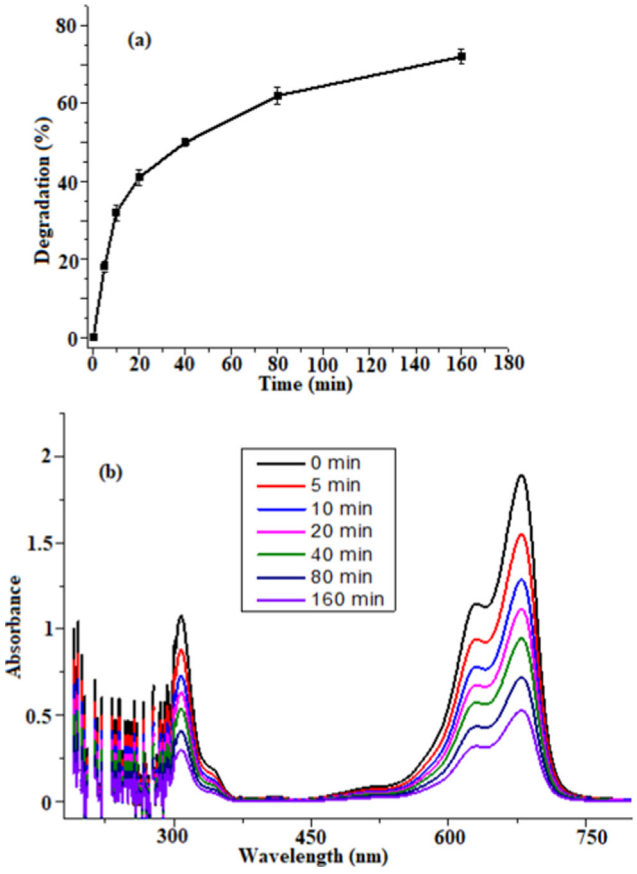

Fig. 9 (a) Degradation (%) of MB w.r.t UV exposure time and (b) UV–visible analysis of MB dye treated isng ZnO NPs catalyst under UB light irradiation.

employed for the photocatalytic removal of MB and Eriochrome black T dyes under direct solar energy expoure. The ZnO NPs displayed auspicious PCA for both dyes removal and up to 92% and 86% efficiency was achieved within 5 h@8.7 $\times$ 10^{-3} and 6.7 $\times$ 10^{-3} (min^{-1}) for MB and ECBT, respectively (Golmohammadi et al., 2020). Similarly, *S. cumini* leaves extracts is employed for the fabrication of ZnO NPs and NPs were in pure crystalline hexagonal and spherical shapes. The ZnO NPs were employed for the removal of RhB dye and under optimum conditions, up to 98% removal of RhB dye was achieved (Rafique et al., 2020). Also, S. baicalensis root extract was employed for ZnO NPs

fabrication, which were studied employing UV–vis, FE-TEM, FTIR, EDX, and XRD approaches. The ZnO NPs displayed auspicious competence for the removal of dye under UV effect with degradation rate of 0.016 min^{-1}, up to 98.6% MB dye was degraded in 210 min (Chen et al., 2019). On the same line, Quince seed mucilage was also employed for the fabrication of ZnO NPs, whose properties were studied by employing FESEM, EDX, FTIR, XRD, UV–Visible techniques. The PCA was appraised for the removal of MB dye and 80% removal was observed within 2 h following the Langmuir–Hinshelwood kinetics model (Tabrizi Hafez Moghaddas et al., 2020). In another study C. sinensis, L. esculentum, C. aurantifolia and C. paradisi peels extracts were tested for the fabrication of ZnO NPs, which were studied by employing XRD, FTIR and HRTEM techniques. The MB dye removal was up to 97% within 180 min irradiation (Nava et al., 2017). Also, *L. nobilis* plant extract furnished ZnO NPs (Wurtzite hexagonal) within 20 and 35 nm range. The ZnO NPs showed promising PCA for RBR-F3B and RR180 dyes under UV light irradiation and up to 99% was achieved in 60 min (Chemingui et al., 2019). Hence, the ZnO prepared utilizing eco-benign approach furnished extremely dynamic photocatalysts and have potential for the remediation of pollutants in the effluents (Abbas et al., 2021; Adetutu et al., 2020; Alaqarbeh et al., 2020; Awwad et al., 2021b; Chham et al., 2018; Elsherif et al., 2021; Shindy et al., 2021; Ukpaka and Eno, 2020) since green route is safer versus other physicochemical approaches (Amer and Awwad, 2021).

$$\text{ZnO NPs} + \text{irradiation} \rightarrow \text{catalyst}(h^+(VB) + e^-(CB)) \quad (5)$$

$$h^+ (VB) + H_2O \rightarrow {}^{\bullet}OH + H^+ \quad (6)$$

$$(CB) + O_2 \rightarrow O^{\bullet}{}_2^- \quad (7)$$

$$O^{\bullet}{}_2^- + 2H^+ \rightarrow HO^{\bullet}{}_2^- + H^+ \rightarrow 2OH^{\bullet} \quad (8)$$

$$OH^{\bullet}/{}^{\bullet}O_2^{-\cdot} + \text{MB dye} \rightarrow CO_2 + H_2O_2 + \text{inorganic ions} \quad (9)$$

3.5. Antibacterial activity

The ABA of ZnO NPs (10–40 mg/L) fabricated using green approach were tested against bacterial strains and responses thus obtained are presented in Fig. 10. The antibacterial in the term of ZOI was recorded to be 17, 19, 21 and 20 (mm) against *E. coli, P. multocida, B. subtilis* and *S. aureus,* respectively at the rate of 10 mg/L ZnO NPs. The ABA was increased significantly with ZnO NPs concentration and ZOI were recorded to be 25 mm (*E. coli*), 24 mm (*P. multocida*), 26 mm (*B. subtilis)* and 26 mm (*S. aureus)*. The ZOI in case of standard drug (Rifampicin) were 33 mm (*E. coli*), 34 mm (*P. multocida*), 36 mm (*B. subtilis)* and 35 mm (*S. aureus)*. In comparison to the standard the ZnO NPs showed promising antibacterial activity. The MIC was also recorded of ZnO NPs against bacterial strains and response this observed are shown in Fig. 11. The MIC values were recorded to be 364, 347, 311 and 321 (μg/L) against *E. coli, P. multocida, B. subtilis* and *S. aureus,* respectively at the rate of 10 mg/L ZnO NPs. The MIC values were decreased as the ZnO NPs concentration was increased and these values were, 215 μg/L (*E. coli*), 231 μg/L

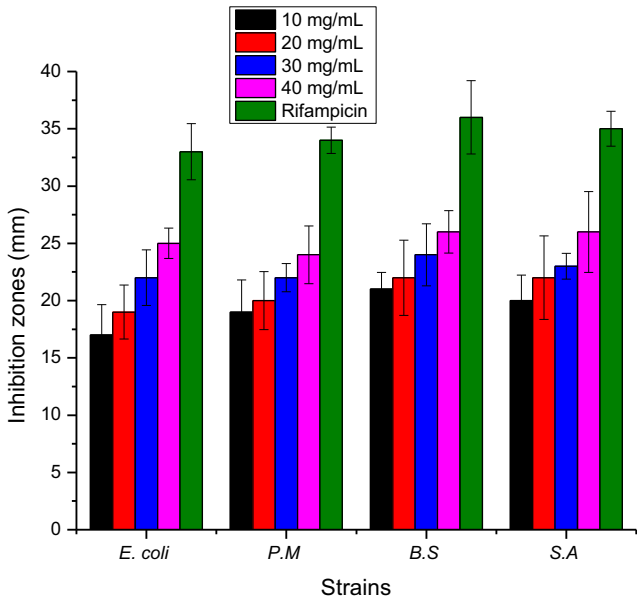

Fig. 10 Zones of inhibition against bacterial strains of ZnO NPs fabricated using *E. japonica* leaves extracts.

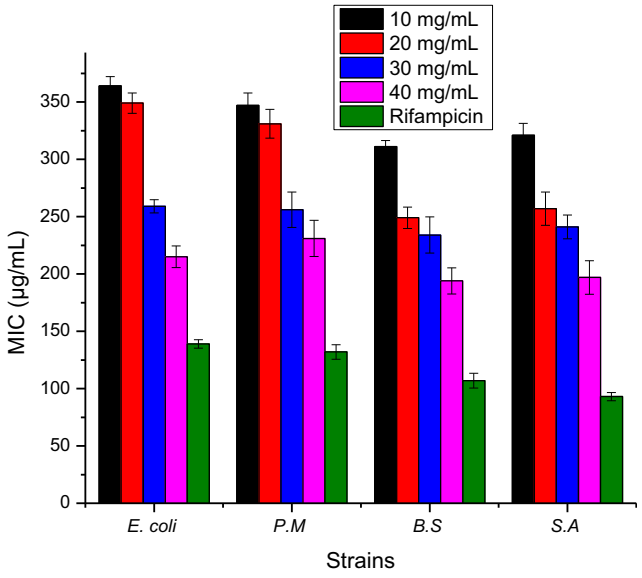

Fig. 11 MIC against bacterial strains of ZnO NPs fabricated using *E. japonica* leaves extracts.

(*P. multocida*), 194 μg/L (*B. subtilis*) and 197 μg/L (*S. aureus*) at the rate of 40 mg/L ZnO NPs. The ZnO NPs interactive bacterial cell wall that cause the destruction of cell wall due to ions and ROS formation (Sharmila et al., 2019).

3.6. Antioxidant activity

The ZnO NPs concentrations (10–40 mg/mL) were employed for DPPH assay to weigh the DPPH (free radical) scavenging activity of ZnO NPs. Ascorbic acid was used as standard for comparison of percentage inhibition of DPPH radical by ZnO NPs. The ZnO NPs displayed excellent inhibition of DPPH radical, which increased as the ZnO NPs increases.

The DPPH is a source of reliable information for antioxidant nature of a substance. High absorbance exhibited high reducing ability (Ahalya et al., 2013). Antioxidants activity measured can be related to bioactive in the extract that intricate the NPs formation from metal ions in the reaction media (Awwad et al., 2020a). The results of DPPH scavenging effect of ZnO NPs (10–40 mg/mL) are given in Fig. 12. The ZnO NPs showed the percentage inhibition of DPPH radical of 36.43 ± 2.46, 56.71 ± 1.35, 68.18 ± 0.76 and 83.23 ± 1.63 for ZnO NPs concentrations (10–40 mg/L), respectively. The TPC and TFC was also evaluated and the outcomes observed are presented in Fig. 13. Both the TPC and TFC contents were increased with concentration and the values were recorded to be in the range of 90.51–315.86 µg GAE/g. DW (TPC) and 48.72–209.34 µg CAE/g. DW (TFC), which revealed a promising antioxidant activity, which is due to bioactive components, which enables the formation NPs (atom) form the metal ions by the reduction process

The observations are in accordance with reported studies that are documented for the ZnO NPs fabrication utilizing eco-benign approaches and their bioactivities, i.e., the ZnO NPs were prepared using *Zea may* husk, jackfruit peel and pomegranate peel, which are characterized and their antimicrobial response was evaluated. The ZnO NPs verified excellent antibacterial activities against *E. faecalis* (Quek et al., 2020). Similarly, P. caerulea fresh leaf extract was employed for ZnO NPs fabrication, which are characterized advanced approaches like FT-IR, SEM, XRD, UV–vis, EDAX and AFM techniques. The ABA was assessed against urinary tract infection causing microbes and ZnO NPs showed promising antibacterial activity (Santhoshkumar et al., 2017). On the same line, ZnO NPs was prepared using *L. nobilis* plant extract. The ZnO NPs indicated promising applications as an active biological agents (Chemingui et al., 2019). The J. regia L. leaf extract has also been used for the fabrication of ZnO NPs as a function of process variable and resultantly, a variables structures and sizes were observed. The antimicrobial effect of ZnO NPs was evaluated against *E.* coli, *P. aeruginosa* and A. baumannii. The antimicrobial effect of ZnO NPs obtained in green route was significantly higher versus chemically synthesized. Also, ZnO NP synthesized using green route was biocompatible versus chemically synthesized (Darvishi et al., 2019). In another study, *C. colocynthis* (L.) extracts were used for ZnO NPs synthesis. The NPs with hexagonal wurtzite structure was in 27–85 nm size range and same were tested for antioxidant and amicrobial activity. The ZnO NPs showed promising antioxidant activity through scavenging of DPPH free radical. *In vitro* cytotoxicity was evaluated against T3 cells and up to 0.26 mg/mL concentration, no toxic effect was observed. The ZnO NPs were highly active *B. subtilis, S. aurous, P. aeruginosa* and *E. coli* bacterial strains. Hence, the present investigation and previous studies proved that green route is efficient method to prepare the ZnO NPs with promising biological activities that might have potential applications in biomedical field (Azizi et al., 2017).

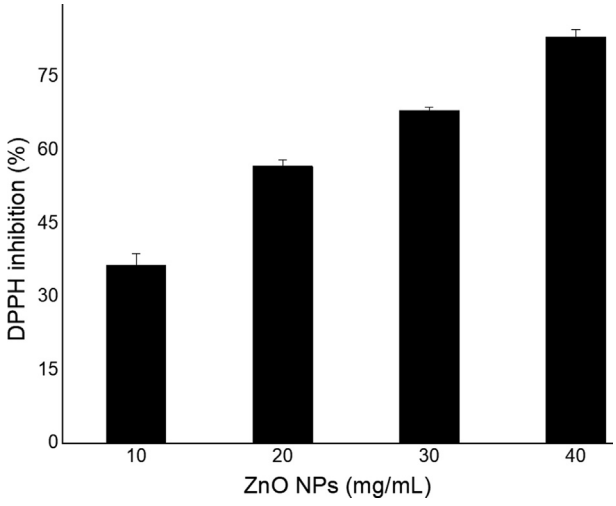

Fig. 12 DPPH radical scavenging activity of ZnO NPs fabricated using *E. japonica* leaves extracts.

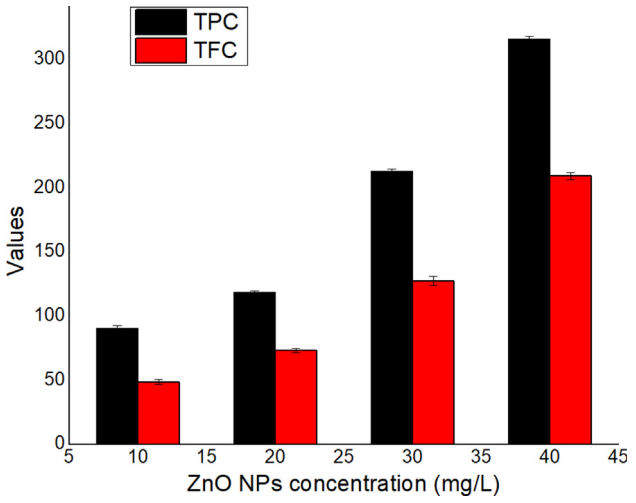

Fig. 13 Value of TPC (total phenolic contents) and TFC (total flavonoid contents).

4. Conclusion

The ZnO NPs was prepared successfully using an eco-benign route, which were studied for different physicochemical properties. The ZnO NPs was highly pure having irregular platelets shape with aggregates tendency and average size was recorded to be 13.0 nm. The antibacterial, antioxidant and photocatalytic activities were also evaluated. The ZnO NPs showed promising DPPH scavenging activity, which was dependent to ZnO NPs concentration. The ZnO NPs was highly active against *E. coli, S. aureus, P. multocida, B. subtilis* strains. The ZnO NPs showed excellent PCA and 160 min of UV irradiation exhibited 72% MB dye degradation. In view of eco-benign and cost effectiveness of green route, the use *E. japonica* extracts is suggested to prepare ZnO NPs for different applications.

Declaration of Competing Interest

The authors declare that they have no known competing financial interests or personal relationships that could have appeared to influence the work reported in this paper.

Acknowledgements

This research was funded by the Deanship of Scientific Research at Princess Nourah bint Abdulrahman University through the Fast-track Research Funding Program.

References

Abbas, M., Hussain, T., Arshad, M., Ansari, A.R., Irshad, A., Nisar, J., Hussain, F., Masood, N., Nazir, A., Iqbal, M., 2019. Wound healing potential of curcumin cross-linked chitosan/polyvinyl alcohol. Int. J. Biol. Macromol. 140, 871–876.

Abbas, N., Butt, M.T., Ahmad, M.M., Deeba, F., Hussain, N., 2021. Phytoremediation potential of Typha latifolia and water hyacinth for removal of heavy metals from industrial wastewater. Chem. Int. 7, 103–111.

Adetutu, I.A., Iwuoha, G.N., Michael Jnr, H., 2020. Carcinogenicity of dioxin-like polychlorinated biphenyls in transformer soil in vicinity of University of Port Harcourt, Choba. Nigeria. Chem. Int. 6, 144–150.

Ahalya, B., Ravishankar, K., PriyaBandhavi, P.J.I., 2013. Evaluation of in vitro anti-oxidant activity of Annona muricata bark. Int. J. Pharma. Chem. Biol. Sci. 3, 406–410.

Al Banna, L.S., Salem, N.M., Jaleel, G.A., Awwad, A.M., 2020. Green synthesis of sulfur nanoparticles using Rosmarinus officinalis leaves extract and nematicidal activity against *Meloidogyne javanica*. Chem. Int. 6, 137–143.

Alaqarbeh, M., Shammout, M., Awwad, A., 2020. Nano platelets kaolinite for the adsorption of toxic metal ions in the environment. Chem. Int. 6, 49–55.

Amer, M.W., Awwad, A.M., 2021. Green synthesis of copper nanoparticles by *Citrus limon* fruits extract, characterization and antibacterial activity. Chem. Int. 7, 1–8.

Arshad, M., Qayyum, A., Shar, G.A., Soomro, G.A., Nazir, A., Munir, B., Iqbal, M., 2018. Zn-doped SiO2 nanoparticles preparation and characterization under the effect of various solvents: Antibacterial, antifungal and photocatlytic performance evaluation. J. Photochem. Photobiol. B 185, 176–183.

Awwad, A.M., Amer, M.W., Salem, N.M., Abdeen, A.O., 2020a. Green synthesis of zinc oxide nanoparticles (ZnO-NPs) using *Ailanthus altissima* fruit extracts and antibacterial activity. Chem. Int. 6, 151–159.

Awwad, A.M., Maisa'a, W., Amer, M.W., 2021a. $Fe(OH)_3$/kaolinite nanoplatelets: Equilibrium and thermodynamic studies for the adsorption of Pb (II) ions from aqueous solution. Chem. Int. 7, 90–102.

Awwad, A.M., Salem, N.M., Amer, M.W., Shammout, M.A.W., 2021b. Adsorptive removal of Pb (II) and Cd (II) ions from aqueous solution onto modified Hiswa iron-kaolin clay: Equilibrium and thermodynamic aspects. Chem. Int. 7, 139–144.

Awwad, A.M., Salem, N.M., Aqarbeh, M.M., Abdulaziz, F.M., 2020b. Green synthesis, characterization of silver sulfide nanoparticles and antibacterial activity evaluation. Chem. Int. 6, 42–48.

Azizi, S., Mohamad, R., Mahdavi Shahri, M., 2017. Green microwave-assisted combustion synthesis of zinc oxide nanoparticles with *Citrullus colocynthis* (L.) Schrad: characterization and biomedical applications. Molecules 22, 301.

Babitha, N., Priya, L.S., Christy, S.R., Manikandan, A., Dinesh, A., Durka, M., Arunadevi, S., 2019. Enhanced antibacterial activity and photo-catalytic properties of ZnO nanoparticles: pedalium murex plant extract-assisted synthesis. J. Nanosci. Nanotechnol. 19, 2888–2894.

Bozin, B., Mimica-Dukic, N., Simin, N., Anackov, G., 2006. Characterization of the volatile composition of essential oils of some Lamiaceae spices and the antimicrobial and antioxidant activities of the entire oils. J. Agric. Food Chem. 54, 1822–1828.

Brudzynski, K., Kim, L., 2011. Storage-induced chemical changes in active components of honey de-regulate its antibacterial activity. Food Chem. 126, 1155–1163.

Chemingui, H., Missaoui, T., Mzali, J.C., Yildiz, T., Konyar, M., Smiri, M., Saidi, N., Hafiane, A., Yatmaz, H., 2019. Facile green synthesis of zinc oxide nanoparticles (ZnO NPs): Antibacterial and photocatalytic activities. Mater. Res. Exp. 6, 1050b1054.

Chen, J., Li, Y., Fang, G., Cao, Z., Shang, Y., Alfarraj, S., Ali Alharbi, S., Li, J., Yang, S., Duan, X., 2021. Green synthesis, characterization, cytotoxicity, antioxidant, and anti-human ovarian cancer activities of Curcumae kwangsiensis leaf aqueous extract green-synthesized gold nanoparticles. Arab. J. Chem. 14, 103000.

Chen, L., Batjikh, I., Hurh, J., Han, Y., Huo, Y., Ali, H., Li, J.F., Rupa, E.J., Ahn, J.C., Mathiyalagan, R., Yang, D.C., 2019. Green synthesis of zinc oxide nanoparticles from root extract of Scutellaria baicalensis and its photocatalytic degradation activity using methylene blue. Optik 184, 324–329.

Chham, A., Khouya, E., Oumam, M., Abourriche, A., Gmouh, S., Mansouri, S., Elhammoudi, N., Hanafi, N., Hannache, H., 2018. The use of insoluble mater of Moroccan oil shale for removal of dyes from aqueous solution. Chem. Int. 4, 67–77.

Chundattu, S.J., Agrawal, V.K., Ganesh, N., 2016. Phytochemical investigation of Calotropis procera. Arab. J. Chem. 9, S230–S234.

Darvishi, E., Kahrizi, D., Arkan, E., 2019. Comparison of different properties of zinc oxide nanoparticles synthesized by the green (using *Juglans regia* L. leaf extract) and chemical methods. J. Mol. Liq. 286, 110831.

Elsherif, K.M., El-Dali, A., Alkarewi, A.A., Mabrok, A., 2021. Adsorption of crystal violet dye onto olive leaves powder: Equilibrium and kinetic studies. Chem. Int. 7, 79–89.

Golmohammadi, M., Honarmand, M., Ghanbari, S., 2020. A green approach to synthesis of ZnO nanoparticles using jujube fruit extract and their application in photocatalytic degradation of organic dyes. Spectrochim. Acta A 229, 117961.

Igwe, O.U., Nwamezie, F., 2018. Green synthesis of iron nanoparticles using flower extract of Piliostigma thonningii and antibacterial activity evaluation. Chem. Int 4, 60–66.

Ismail, R.M., Almaqtri, W.Q., Hassan, M., 2021. Kaolin and bentonite catalysts efficiencies for the debutylation of 2-tert-butylphenol. Chem. Int. 7, 21–29.

Jabeen, S., Ali, S., Nadeem, M., Arif, K., Qureshi, N., Shar, G.A., Soomro, G.A., Iqbal, M., Nazir, A., Siddiqua, U.H., 2019. Statistical Modeling for the Extraction of Dye from Natural Source and Industrial Applications. Polish J. Environ. Stud. 28, 2145–2150.

Jamdagni, P., Khatri, P., Rana, J.S., 2018. Green synthesis of zinc oxide nanoparticles using flower extract of Nyctanthes arbor-tristis and their antifungal activity. J. King Saud Uni.- Sci. 30, 168–175.

Jamil, A., Bokhari, T.H., Javed, T., Mustafa, R., Sajid, M., Noreen, S., Zuber, M., Nazir, A., Iqbal, M., Jilani, M.I., 2020. Photocatalytic degradation of disperse dye Violet-26 using TiO_2 and ZnO nanomaterials and process variable optimization. J. Mater. Res. Technol. 9, 1119–1128.

Jamila, N., Khan, N., Bibi, A., Haider, A., Noor Khan, S., Atlas, A., Nishan, U., Minhaz, A., Javed, F., Bibi, A., 2020. Piper longum catkin extract mediated synthesis of Ag, Cu, and Ni nanoparticles and their applications as biological and environmental remediation agents. Arab. J. Chem. 13, 6425–6436.

Kamran, U., Bhatti, H.N., Iqbal, M., Nazir, A., 2019. Green Synthesis of Metal Nanoparticles and their Applications in Different Fields: A Review. Z. Phys. Chem. 233, 1325–1349.

Khan, N.-U.-H., Bhatti, H.N., Iqbal, M., Nazir, A., Ain, H., 2020. Kinetic Study of Degradation of Basic Turquise Blue X-GB and Basic Blue X-GRRL using Advanced Oxidation Process. Z. Phys. Chem. 234, 1803–1817.

Khan, N.U.-H., Bhatti, H.N., Iqbal, M., Nazir, A., 2019. Decolorization of Basic Turquise Blue X-GB and Basic Blue X-GRRL by the Fenton's Process and its Kinetics. Z. Phys. Chem. 233, 361–373.

Li, F., Li, Y., Li, Q., Shi, X., 2020. Eriobotrya japonica leaf triterpenoid acids ameliorate metabolic syndrome in C57BL/6J mice fed with high-fat diet. Biomed. Pharmacother. 132, 110866.

Li, S., Al-Misned, F.A., El-Serehy, H.A., Yang, L., 2021. Green synthesis of gold nanoparticles using aqueous extract of Mentha Longifolia leaf and investigation of its anti-human breast carcinoma properties in the in vitro condition. Arab. J. Chem. 14, 102931.

Mahmud, R.A., Shafawi, A.N., Ahmed Ali, K., Putri, L.K., Md Rosli, N.I., Mohamed, A.R., 2020. Graphene nanoplatelets with low defect density as a synergetic adsorbent and electron sink for ZnO in the photocatalytic degradation of Methylene Blue under UV–vis irradiation. Mater. Res. Bull. 128, 110876.

Mathew, S., Victório, C.P., Sidhi, J., BH, B.T., 2020. Biosynthesis of silver nanoparticle using flowers of *Calotropis gigantea* (L.) W.T. Aiton and activity against pathogenic bacteria. Arab. J. Chem. 13, 9139–9144.

Mukhtar, A., Ghulam, A., Rizwan, H., Fatima, J., Ghulam Abbas, S., Gul Afshan, S., Naseem, Q., Munawar, I., Arif, N., 2019. Kinetics and equilibrium studies of eriobotrya japonica: a novel adsorbent preparation for dyes sequestration. Z. Phys. Chem. 233, 1469–1484.

Nava, O.J., Soto-Robles, C.A., Gómez-Gutiérrez, C.M., Vilchis-Nestor, A.R., Castro-Beltrán, A., Olivas, A., Luque, P.A., 2017. Fruit peel extract mediated green synthesis of zinc oxide nanoparticles. J. Mol. Struct. 1147, 1–6.

Numrah, N., Omamah, A., Atif, I., Aftab, A., Muhammd, Y., Abdul, G., Munawar, I., Arif, N., Nasir, M., 2019. A novel approach for modification of biosorbent by silane functionalization and its industrial application for single and multi-component solute system. Z. Phys. Chem. 233, 1603–1623.

Padalia, H., Chanda, S., 2017. Characterization, antifungal and cytotoxic evaluation of green synthesized zinc oxide nanoparticles using Ziziphus nummularia leaf extract. Artificial Cells. Nanomed. Biotechnol. 45, 1751–1761.

Quek, J.-A., Sin, J.-C., Lam, S.-M., Mohamed, A.R., Zeng, H., 2020. Bioinspired green synthesis of ZnO structures with enhanced visible light photocatalytic activity. J. Mater. Sci.: Mater. Electron. 31, 1144–1158.

Rafique, M., Tahir, R., Gillani, S.S.A., Tahir, M.B., Shakil, M., Iqbal, T., Abdellahi, M.O., 2020. Plant-mediated green synthesis of zinc oxide nanoparticles from Syzygium Cumini for seed germination and wastewater purification. Int. J. Environ. Anal. Chem. 26, 1–16.

Remya, V., Abitha, V., Rajput, P., Rane, A., Dutta, A., 2017. Silver nanoparticles green synthesis: a mini review. Chem. Int. 3, 165–171.

Rupa, E.J., Kaliraj, L., Abid, S., Yang, D.-C., Jung, S.-K., 2019. Synthesis of a zinc oxide nanoflower photocatalyst from sea buckthorn fruit for degradation of industrial dyes in wastewater treatment. Nanomaterials 9, 1692.

Sakanaka, S., Tachibana, Y., Okada, Y., 2005. Preparation and antioxidant properties of extracts of Japanese persimmon leaf tea (kakinoha-cha). Food Chem. 89, 569–575.

Sanda, M.D.A., Badu, M., Awudza, J.A., Boadi, N.O., 2021. Development of TiO_2-based dye-sensitized solar cells using natural dyes extracted from some plant-based materials. Chem. Int. 7, 9–20.

Santhoshkumar, J., Kumar, S.V., Rajeshkumar, S., 2017. Synthesis of zinc oxide nanoparticles using plant leaf extract against urinary tract infection pathogen. Resourc. Efficient Technol. 3, 459–465.

Sarker, S.D., Nahar, L., Kumarasamy, Y., 2007. Microtitre plate-based antibacterial assay incorporating resazurin as an indicator of cell growth, and its application in the in vitro antibacterial screening of phytochemicals. Methods 42, 321–324.

Shammout, M.W., Awwad, A.M., 2021. A novel route for the synthesis of copper oxide nanoparticles using Bougainvillea plant flowers extract and antifungal activity evaluation. Chem. Int. 7, 71–78.

Sharmila, G., Thirumarimurugan, M., Muthukumaran, C., 2019. Green synthesis of ZnO nanoparticles using Tecoma castanifolia leaf extract: Characterization and evaluation of its antioxidant, bactericidal and anticancer activities. Microchem. J. 145, 578–587.

Shindy, H.A., El-Maghraby, M.A., Eissa, F.M., 2021. Solvatochromism and halochromism of some furo/pyrazole cyanine dyes. Chem. Int. 7, 39–52.

Sidik, D.A.B., Hairom, N.H.H., Mohammad, A.W., Halim, N.A., Ahmad, M.K., Hamzah, S., Sulaiman, N., 2020. The potential control strategies of membrane fouling and performance in membrane photocatalytic reactor (MPR) for treating palm oil mill secondary effluent (POMSE). Chem. Eng. Res. Design 162, 12–27.

Sohail, I., Bhatti, I.A., Ashar, A., Sarim, F.M., Mohsin, M., Naveed, R., Yasir, M., Iqbal, M., Nazir, A., 2020. Polyamidoamine (PAMAM) dendrimers synthesis, characterization and adsorptive removal of nickel ions from aqueous solution. J. Mater. Res. Technol. 9, 498–506.

Sönmezoğlu, S., Eskizeybek, V., Toumiat, A., Avcı, A., 2014. Fast production of ZnO nanorods by arc discharge in de-ionized water and applications in dye-sensitized solar cells. J. Alloy. Comp. 586, 593–599.

Tabrizi Hafez Moghaddas, S.M., Elahi, B., Javanbakht, V., 2020. Biosynthesis of pure zinc oxide nanoparticles using Quince seed mucilage for photocatalytic dye degradation. J. Alloy. Comp. 821, 153519.

Ukpaka, C.P., Eno, O.N., 2020. Modeling of Azadirachta indica leaves powder efficiency for the remediation of soil contaminated with crude oil. Chem. Int. 7, 62–70.

Varadavenkatesan, T., Lyubchik, E., Pai, S., Pugazhendhi, A., Vinayagam, R., Selvaraj, R., 2019. Photocatalytic degradation of Rhodamine B by zinc oxide nanoparticles synthesized using the leaf extract of *Cyanometra ramiflora*. J. Photochem. Photobiol. B 199, 111621.

Weldegebrieal, G.K., 2020. Synthesis method, antibacterial and photocatalytic activity of ZnO nanoparticles for azo dyes in wastewater treatment: A review. Inorgan. Chem. Commun. 120, 108140.

Yedurkar, S., Maurya, C., Mahanwar, P., 2016. Biosynthesis of zinc oxide nanoparticles using ixora coccinea leaf extract—a green approach. Open J. Synth. Theor. Appl. 5, 1–14.